Cholera Transmission Dynamics with Sanitation Control Measures

Abdallah Alsammani*[1], Gassan A.M.O. Farah[2,3], Mohammed A.Y. Mohammed[4], and Mehmet Yavuz[5,6]

[1]Department of Mathematics, Jacksonville University, Jacksonville, FL, USA
[2]Department of Mathematics and Applied Mathematics, University of Western Cape, South Africa
[3]Department of Mathematics and Physics, Cape Peninsula University of Technology, Bellville, South Africa
[4]Department of Mathematics and Statistics, Georgia State University, Atlanta, GA, USA
[5]Department of Mathematics and Computer Sciences, Necmettin Erbakan University, Konya, Türkiye
[6]Department of Applied Mathematics and Informatics, Kyrgyz-Turkish Manas University, Bishkek, Kyrgyzstan

Abstract

Cholera remains a significant public health challenge globally, particularly affecting regions with inadequate water, sanitation, and hygiene infrastructures. This study presents a comprehensive mathematical model extending the classical Susceptible-Infected-Recovered (SIR) model by explicitly incorporating both direct human-to-human and indirect environment-to-human transmission routes of *Vibrio cholerae*. The proposed model systematically integrates three primary intervention strategies—human sanitation, environmental sanitation, and vaccination. We derive the basic reproduction number ($\mathcal{R}_0$) through rigorous mathematical analyses and establish stability conditions for disease-free and endemic equilibria. Numerical simulations underscore the superior Efficacy of combined intervention approaches, demonstrating significant reductions in infection prevalence and epidemic duration compared to singular strategies. Sensitivity and bifurcation analyses highlight the critical influence of environmental transmission parameters, emphasizing water treatment's pivotal role in effective cholera prevention. This study provides a robust quantitative basis for formulating optimized, context-specific cholera control policies, particularly suited for implementation in resource-limited settings.

Keywords: *Cholera modeling, Environmental transmission, Human sanitation, Vaccination strategy, Bifurcation analysis, Sensitivity analysis, Mathematical epidemiology.*

1 Introduction

Cholera, an acute diarrhoeal infection caused by ingestion of the bacterium *Vibrio cholerae*, continues to pose a significant global public health challenge, particularly in regions with inadequate Water, Sanitation, and Hygiene (WASH) infrastructure. Epidemiological data from the World Health Organization indicates that cholera affects approximately 1.3 to 4 million individuals annually, resulting in an estimated 21,000 to 143,000 fatalities worldwide [20]. The persistence of cholera outbreaks in low-resource settings underscores the limitations of current

*Corresponding author: aalsamm@ju.edu

preventive interventions. It highlights the critical necessity for developing more effective, sustainable control strategies to mitigate this preventable disease burden.

Cholera transmission occurs through both direct interpersonal contact and indirect exposure to contaminated environmental reservoirs, particularly polluted water sources, which presents significant challenges for disease eradication initiatives [19]. Effective outbreak control strategies necessitate the simultaneous implementation of ecological sanitation improvements and behavioral interventions at the community level. Mathematical modeling serves as an essential analytical framework for elucidating cholera transmission dynamics and evaluating the Efficacy of public health interventions [11].

Epidemiologists have extensively employed compartmental models to elucidate pathogen dynamics and evaluate public health intervention efficacy [4, 10]. The foundational Susceptible-Infected-Recovered (SIR) framework has served as an instrumental analytical tool for investigating transmission patterns in diseases such as influenza [12] and measles [13]. Cholera transmission, however, with its distinctive environmental contamination pathway, demands more sophisticated modeling approaches. Pioneering cholera models expanded the conventional SIR architecture by incorporating an ecological reservoir component, thereby acknowledging the critical role of contaminated water sources in disease propagation [8].

The transmission of cholera occurs through two distinct pathways: direct human-to-human contact and indirect environmental exposure via contaminated water sources, creating significant challenges for disease eradication initiatives [19]. Effectively controlling outbreaks requires multifaceted approaches integrating ecological sanitation improvements with behavioral interventions. Mathematical modeling has emerged as an essential analytical framework in this domain, providing critical insights into transmission dynamics and enabling rigorous evaluation of public health intervention efficacy [11].

The SIWR (Susceptible-Infected-Water-Recovered) model establishes a comprehensive mathematical framework for cholera epidemiology by explicitly incorporating pathogen dynamics within environmental water reservoirs [6]. This sophisticated approach enables quantitative assessment of intervention efficacy, including water treatment protocols and vaccination campaigns, on the basic reproduction number $\mathcal{R}_0$ and subsequent outbreak potential. Empirical investigations employing the SIWR model have consistently demonstrated that enhancements to sanitation infrastructure and water quality result in significant reductions in $\mathcal{R}_0$, thereby substantially decreasing the probability of widespread epidemic transmission [23, 14]

Comprehensive evaluations of multifaceted intervention approaches have become increasingly prominent in contemporary modeling research. Empirical evidence demonstrates that integrated strategies combining vaccination protocols with water, sanitation, and hygiene (WASH) improvements yield significantly enhanced reductions in cholera transmission rates compared to implementations of isolated interventions. These observations underscore the need to develop context-specific, integrated frameworks that account for local epidemiological patterns and resource constraints in regions characterized by high cholera endemicity [5, 1].

Mathematical models originally developed for a wide range of infectious diseases provide powerful theoretical foundations that can be effectively adapted to enhance cholera intervention strategies. For instance, studies on vector-borne diseases such as malaria [22] and dengue [16] have highlighted the critical role of environmental management in controlling transmission. Similarly, research on respiratory infections, particularly COVID19 has demonstrated the effectiveness of non-pharmaceutical interventions (NPIs) in significantly curbing the spread of disease [24, 3]. These insights align with broader trends in epidemiological modeling, including

recent applications of stochastic frameworks for infection dynamics [2] and complex ecological interactions [17], offering a rich foundation for informing cholera control policies.

This study advances cholera transmission modeling through a comprehensive framework integrating behavioral factors, environmental determinants, and intervention synergies. Extending the traditional SIWR paradigm, our model accounts for both human-to-human and environment-to-human transmission pathways of *Vibrio cholerae*. We incorporate human sanitation, environmental sanitation, and vaccination strategies while deriving the basic reproduction number ($\mathcal{R}_0$) to establish equilibria stability conditions. Analysis of South African outbreak data demonstrates that combined interventions significantly outperform singular approaches. Sensitivity analyses reveal the predominant influence of environmental transmission parameters, emphasizing water treatment's pivotal role in cholera prevention. This research provides quantitative foundations for developing context-specific control policies in resource-constrained settings.

2 Model Formulation

We consider a human population subdivided into three epidemiological compartments: The population includes susceptible individuals ($S(t)$), infected individuals ($I(t)$), and those who have recovered from infection ($R(t)$). The total population size $N(t)$ at time t consists of the sum of susceptible individuals $S(t)$, infected individuals $I(t)$, and recovered individuals $R(t)$ as shown by $N(t) = S(t) + I(t) + R(t)$. Cholera infection spreads through contact with infected people and exposure to contaminated environmental resources like water sources. At any given time t, the environmental pathogen concentration $W(t)$ provides the measurement.

Transmission occurs through two main routes: Cholera spreads between humans at a β_1 rate through contact and from environmental contamination level $W(t)$. The pattern of environmental transmission to human hosts obeys a Monod-type saturation function [18], which defines the nonlinear connection between pathogen concentration and infection speed. Specifically, we define

$$\beta_2(W) = \beta_{\max} \frac{W}{k + W},$$

$\beta_{\max}$ represents the maximum environment-to-human transmission rate and k signifies the half-saturation constant. The transmission rate achieves a maximum limit as W increases, with the function preventing it from becoming limitless.

The recovery rate for each infected person is γ, which results in an average infectious period of $1/\gamma$. Every person starts life in the susceptible class at rate Λ and experiences natural death at rate μ. The death rate due to disease is represented by δ, which shows the connection between infection and increased mortality.

Basic cholera models [15, 9, 21] demonstrate that infected people contribute to rising environmental pathogen levels through shedding pathogen θ. Pathogen concentration decays at a rate of σ when shedding stops, which stops $W(t)$ from building up endlessly. The linear assumption demonstrates that environmental contamination rises with infection levels but declines when pathogen concentration increases.

The model includes public health interventions to evaluate their collective effect in preventing disease spread. Two key measures are considered: human sanitation and environmental sanitation. The direct human-to-human transmission rate drops by $(1 - \epsilon_h)$ when human sanitation measures are applied, and ϵ_h represents their effectiveness as $0 \leq \epsilon_h \leq 1$. The effectiveness

of environmental sanitation interventions such as water purification and waste disposal diminishes the environment-to-human transmission rate by $(1-\epsilon_w)$ where the efficacy rate ϵ_w varies between 0 and 1. The model includes the possibility that susceptible individuals receive vaccinations at rate ν, which grants them immunity, moving them directly to the recovered class without first becoming infected.

Combining these assumptions, we obtain the following system of nonlinear ordinary differential equations describing cholera transmission dynamics:

$$\begin{aligned}
\frac{dS}{dt} &= \Lambda - \beta_1(1-\epsilon_h)\frac{I}{N}S - \beta_2(W)(1-\epsilon_w)S - (\mu+\nu)S,\\
\frac{dI}{dt} &= \beta_1(1-\epsilon_h)\frac{I}{N}S + \beta_2(W)(1-\epsilon_w)S - (\gamma+\mu+\delta)I,\\
\frac{dR}{dt} &= \gamma I + \nu S - \mu R,\\
\frac{dW}{dt} &= \theta I - \sigma W.
\end{aligned} \tag{1}$$

These equations are complemented by the initial conditions $S(0) = S^0 > 0$, $I(0) = I^0 > 0$, $R(0) = 0$, and $W(0) = W^0 > 0$.

Our analysis focuses on understanding the qualitative dynamics of this model and the conditions under which cholera outbreaks can be prevented or mitigated through the combination of control measures. Both analytical approaches (e.g., stability analysis of equilibria) and numerical simulations (using `ode45` in MATLAB) are employed to explore the model's behavior under various parameter scenarios.

Table 1: Model Variables and Parameters

Variable	**Description**
$S(t)$	Susceptible population at time t
$I(t)$	Infected population at time t
$R(t)$	Recovered population at time t
$W(t)$	Pathogen concentration in the environment at time t
Parameter	
Λ	Recruitment (birth) rate of susceptibles
μ	Natural mortality rate
δ	Disease-induced mortality rate
γ	Recovery rate from infection
β_1	Direct human-to-human transmission rate
$\beta_{\max}$	Maximal environment-to-human transmission rate
k	Half-saturation constant for pathogen concentration
θ	PathoPathogending rate by infected individuals
σ	Pathogen decay/removal rate in the environment
ϵ_h	Efficacy of human sanitation (0–1)
ϵ_w	Efficacy of environmental sanitation (0–1)
ν	Vaccination rate

2.1 Existence, Uniqueness, and Positivity of Solutions

Before analyzing the qualitative behavior of the model, it is essential to establish the fundamental properties of the solution trajectories, including existence, uniqueness, and positivity.

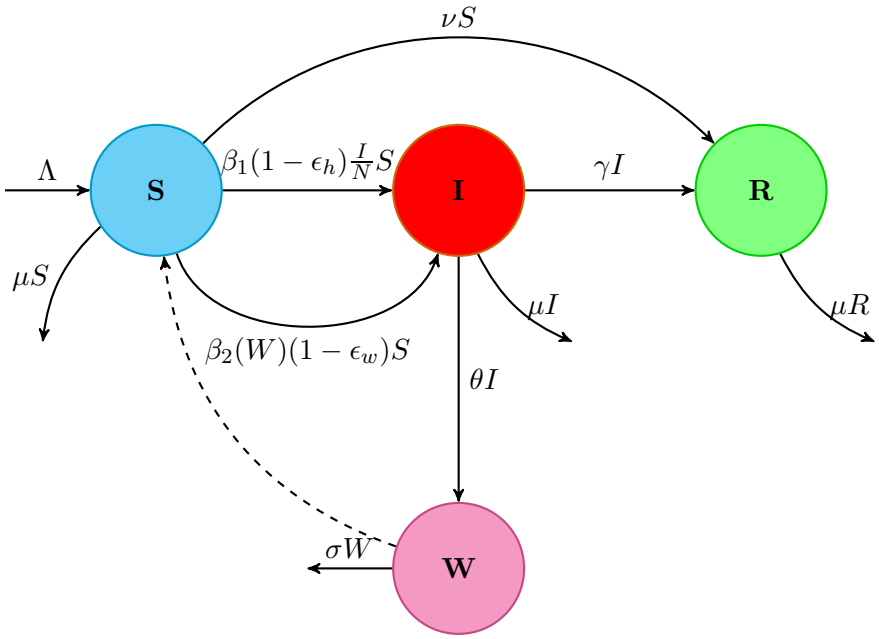

Figure 1: Compartmental model of cholera transmission dynamics with human and environmental interactions. The model illustrates four compartments: Susceptible (S), Infected (I), Recovered (R), and environmental pathogen concentration (W). Arrows indicate the flow between compartments with their corresponding rates. Direct human-to-human transmission ($\beta_1(1-\epsilon_h)\frac{I}{N}S$) and environment-to-human transmission ($\beta_2(W)(1-\epsilon_w)S$) are shown, along with public health interventions through human sanitation (ϵ_h) and environmental sanitation (ϵ_w) parameters. Other processes include vaccination (νS), recovery (γI), pathogen shedding (θI), environmental decay (σW), recruitment (Λ), and mortality (μ).

In this section, we prove that, given nonnegative initial conditions, the system of equations (1) admits a unique, continuously differentiable solution that remains positive for all future times.

Existence and Uniqueness of Solutions

Consider the system 1 and define the state vector.

$$\mathbf{x}(t) = \big(S(t), I(t), R(t), W(t)\big)^\top.$$

The right-hand side of the system can be written as a function $\mathbf{f} : \mathbb{R}^4 \to \mathbb{R}^4$, where

$$\mathbf{f}(S,I,R,W) = \begin{pmatrix} \Lambda - \beta_1(1-\epsilon_h)\frac{I}{S+I+R}S - \beta_2(W)(1-\epsilon_w)S - (\mu+\nu)S \\ \beta_1(1-\epsilon_h)\frac{I}{S+I+R}S + \beta_2(W)(1-\epsilon_w)S - (\gamma+\mu+\delta)I \\ \gamma I + \nu S - \mu R \\ \theta I - \sigma W \end{pmatrix}.$$

We assume that all parameters are nonnegative and finite. Moreover, $\beta_2(W)$ is given by a Monod function:

$$\beta_2(W) = \beta_{\max}\frac{W}{k+W},$$

Whichh is continuously differentiable concerning W for $W \geq 0$. Since all other terms are linear or rational functions of S, I, R, W and are continuously differentiable in their domains, it follows that $\mathbf{f}$ is locally Lipschitz continuous in $\mathbb{R}^4$.

Theorem 2.1 (Local Existence and Uniqueness)**.** *For any initial condition* $\mathbf{x}(0) = (S^0, I^0, R^0, W^0) \in \mathbb{R}^4_{\geq 0}$*, there exists a unique, maximal solution* $\mathbf{x}(t)$ *to the system of equations* (1) *defined on some maximal interval* $[0, T_{\max})$ *with* $T_{\max} > 0$*.*

Proof. By the standard theory of ordinary differential equations (e.g., Picard–Lindelöf theorem [7]), local existence and uniqueness of solutions follow from the fact that $\mathbf{f}$ is continuous and locally Lipschitz in $\mathbf{x}$. Since all parameter values are assumed to be finite and nonnegative, and the functions are at least continuously differentiable in the relevant domain, the conditions for the existence-uniqueness theorem are satisfied. Therefore, a unique local solution exists. □

Positivity of Solutions

Next, if the initial conditions are nonnegative, the solutions remain in the nonnegative orthant for all $t \geq 0$. In epidemiological models, this property ensures that variables representing populations and pathogen concentrations do not become negative, which is biologically meaningful.

Theorem 2.2 (Positivity Invariance)**.** *Suppose* $S^0 \geq 0$*,* $I^0 \geq 0$*,* $R^0 \geq 0$*, and* $W^0 \geq 0$*. Then, for all* $t \geq 0$ *for which the solution exists, we have* $S(t) \geq 0$*,* $I(t) \geq 0$*,* $R(t) \geq 0$*, and* $W(t) \geq 0$*.*

Proof. We proceed by contradiction and a componentwise argument.

Nonnegativity of $S(t)$: Assume there exists a time $t_1 > 0$ such that $S(t)$ is the first component to become negative. Since $S(0) = S^0 \geq 0$, continuity ensures $S(t) \geq 0$ for all $0 \leq t < t_1$ and $S(t_1) = 0$. Differentiating at t_1,

$$\left.\frac{dS}{dt}\right|_{t=t_1} = \Lambda - \beta_1(1-\epsilon_h)\frac{I(t_1)}{N(t_1)}S(t_1) - \beta_2(W(t_1))(1-\epsilon_w)S(t_1) - (\mu+\nu)S(t_1).$$

Since $S(t_1) = 0$, the terms involving $S(t_1)$ vanish, leaving

$$\left.\frac{dS}{dt}\right|_{t=t_1} = \Lambda > 0.$$

This indicates that its derivative is positive when $S(t)$ hits zero. Thus, $S(t)$ cannot cross zero and become harmful. Therefore, $S(t)$ remains nonnegative for all $t \geq 0$.

Nonnegativity of $I(t)$: Similarly, assume $I(t)$ becomes negative at some time $t_2 > 0$ for the first time. By the same continuity argument, $I(t) \geq 0$ for $0 \leq t < t_2$ and $I(t_2) = 0$. Then

$$\left.\frac{dI}{dt}\right|_{t=t_2} = \beta_1(1-\epsilon_h)\frac{I(t_2)}{N(t_2)}S(t_2) + \beta_2(W(t_2))(1-\epsilon_w)S(t_2) - (\gamma+\mu+\delta)I(t_2).$$

Since $I(t_2) = 0$, the only terms surviving are $\beta_2(W(t_2))(1-\epsilon_w)S(t_2)$, because $I(t_2) = 0$ zeroes out the first and last terms. Given $S(t_2) \geq 0$ and $W(t_2) \geq 0$, we have $\beta_2(W(t_2)) \geq 0$, so

$$\left.\frac{dI}{dt}\right|_{t=t_2} = \beta_2(W(t_2))(1-\epsilon_w)S(t_2) \geq 0.$$

In fact, if $S(t_2) > 0$ and $W(t_2) > 0$, then this derivative is strictly positive, preventing $I(t)$ from decreasing below zero. If $S(t_2) = 0$, then as shown above, $S(t)$ is nonnegative and will not become negative, and similarly for $W(t_2)$. Thus, $I(t)$ cannot become negative, and it follows that $I(t) \geq 0$ for all $t \geq 0$.

Nonnegativity of $R(t)$: For $R(t)$, suppose it becomes negative at some time $t_3 > 0$. Then $R(t_3) = 0$. We have

$$\left.\frac{dR}{dt}\right|_{t=t_3} = \gamma I(t_3) + \nu S(t_3) - \mu R(t_3) = \gamma I(t_3) + \nu S(t_3) \geq 0,$$

since $I(t_3) \geq 0$ and $S(t_3) \geq 0$ have been established. Thus, $R(t)$ cannot decrease through zero and become negative. Hence $R(t) \geq 0$ for all $t \geq 0$.

Nonnegativity of $W(t)$: Finally, consider $W(t)$. Suppose $W(t)$ becomes negative at some time $t_4 > 0$. Then $W(t_4) = 0$. Evaluating its derivative,

$$\left.\frac{dW}{dt}\right|_{t=t_4} = \theta I(t_4) - \sigma W(t_4) = \theta I(t_4) \geq 0,$$

since $I(t_4) \geq 0$ and $\sigma > 0$. Thus, $W(t)$ also cannot become negative.

Combining these arguments, we conclude that if the initial conditions are nonnegative, the solution remains nonnegative in all components for as long as it exists. □

Global Existence

By standard comparison arguments and the fact that the population and the pathogen concentration are modeled with realistic birth, death, and decay processes, the state variables cannot blow up in finite time. Specifically, no finite-time singularities occur because the birth and mortality processes are linear, and the pathogen concentration W is governed by a linear input from I and a linear decay term. Moreover, the total population $N(t) = S(t) + I(t) + R(t)$ is bounded from above by a solution to a linear ODE (since births and deaths are bounded), and $W(t) a linear ODE similarly bounds$ with nonnegative initial conditions.

Hence, standard ODE theory (see [7]) implies that the maximal interval of existence $[0, T_{\max})$ can be extended indefinitely (since no blow-up occurs), ensuring that $T_{\max} = +\infty$. Thus, solutions are globally defined for all $t \geq 0$.

Theorem 2.3 (Global Existence of Solutions)**.** *Given nonnegative initial conditions, the unique solution of the system 1 exists for all $t \geq 0$ and remains in $\mathbb{R}^4 \geq 0$.*

Proof. Local existence and uniqueness have been established. The positivity of the solutions prevents the population or pathogen concentration from becoming negative. The boundedness of birth and death terms, combined with the linear decay in pathogen concentration, ensures no finite-time blow-up. Thus, by standard extension arguments in ODE theory [7], the solution is extendable to all $t \geq 0$. □

3 Mathematics Analysis

3.1 Equilibrium Solutions

3.2 Disease-Free and Endemic Equilibria

In this section, we derive the disease-free equilibrium (DFE) and discuss the conditions leading to an endemic equilibrium (EE) for the system 1.

Disease-Free Equilibrium (DFE)

Disease-free equilibrium occurs when there is no infection in the population. Hence, at the DFE, we set:

$$I^* = 0, \quad W^* = 0.$$

Substitute $I^* = 0$ and $W^* = 0$ into the equilibrium conditions.

1. From $\frac{dW}{dt} = 0$:

$$0 = \theta I^* - \sigma W^* \implies 0 = \theta \cdot 0 - \sigma \cdot 0,$$

Which is satisfied trivially.

2. From $\frac{dR}{dt} = 0$ and using $I^* = 0$:

$$0 = \gamma \cdot 0 + \nu S^* - \mu R^* \implies \nu S^* = \mu R^* \implies R^* = \frac{\nu}{\mu} S^*.$$

3. From $\frac{dS}{dt} = 0$ and using $I^* = 0$, $W^* = 0$:

$$0 = \Lambda - (\mu + \nu) S^*,$$

since the terms involving I^* and W^* vanish. Thus,

$$S^* = \frac{\Lambda}{\mu + \nu}.$$

4. Given $R^* = \frac{\nu}{\mu} S^*$, substitute $S^* = \frac{\Lambda}{\mu+\nu}$:

$$R^* = \frac{\nu}{\mu} \cdot \frac{\Lambda}{\mu + \nu}.$$

Therefore, the DFE is:

$$(S^*, I^*, R^*, W^*) = \left(\frac{\Lambda}{\mu + \nu},\, 0,\, \frac{\nu \Lambda}{\mu(\mu + \nu)},\, 0 \right).$$

Endemic Equilibrium (EE)

The endemic equilibrium (EE) is characterized by the presence of infection in the population, implying $I^* > 0$ and $W^* > 0$. At equilibrium, we still have:

$$\frac{dS}{dt} = 0, \quad \frac{dI}{dt} = 0, \quad \frac{dR}{dt} = 0, \quad \frac{dW}{dt} = 0.$$

1. From $\frac{dW}{dt} = 0$:

$$0 = \theta I^* - \sigma W^* \implies W^* = \frac{\theta}{\sigma} I^*.$$

Thus, the environmental pathogen concentration is directly proportional to the number of infected individuals at equilibrium.

2. From $\frac{dR}{dt} = 0$:

$$0 = \gamma I^* + \nu S^* - \mu R^* \implies R^* = \frac{\gamma I^* + \nu S^*}{\mu}.$$

3. We now have expressions for R^* and W^* in terms of S^* and I^*. The total population at equilibrium is:

$$N^* = S^* + I^* + R^* = S^* + I^* + \frac{\gamma I^* + \nu S^*}{\mu}.$$

It follows that

$$N^* = S^* \left(1 + \frac{\nu}{\mu}\right) + I^* \left(1 + \frac{\gamma}{\mu}\right).$$

4. Consider the $\frac{dI}{dt} = 0$ equation at equilibrium:

$$0 = \beta_1(1 - \epsilon_h)\frac{I^*}{N^*} S^* + \beta_2(W^*)(1 - \epsilon_w)S^* - (\gamma + \mu + \delta)I^*.$$

Since $I^* > 0$, we can divide through by I^*:

$$0 = \beta_1(1 - \epsilon_h)\frac{S^*}{N^*} + \frac{\beta_2(W^*)(1 - \epsilon_w)S^*}{I^*} - (\gamma + \mu + \delta).$$

Using $W^* = \frac{\theta}{\sigma} I^*$, we get:

$$\beta_2(W^*) = \beta_{\max}\frac{W^*}{k + W^*} = \beta_{\max}\frac{\frac{\theta}{\sigma} I^*}{k + \frac{\theta}{\sigma} I^*}.$$

Thus:

$$(\gamma + \mu + \delta) = \beta_1(1 - \epsilon_h)\frac{S^*}{N^*} + (1 - \epsilon_w)S^* \frac{\beta_{\max}\frac{\theta}{\sigma} I^*}{I^*(k\frac{\sigma}{\theta} + I^*)}.$$

Simplify the second term. Notice that the I^* cancels:

$$(\gamma + \mu + \delta) = \beta_1(1 - \epsilon_h)\frac{S^*}{N^*} + (1 - \epsilon_w)\frac{\beta_{\max}\theta S^*}{\sigma(k + \frac{\theta}{\sigma} I^*)}.$$

5. Consider the $\frac{dS}{dt} = 0$ equation at equilibrium:

$$0 = \Lambda - (\mu + \nu)S^* - \beta_1(1 - \epsilon_h)\frac{I^*}{N^*}S^* - \beta_2(W^*)(1 - \epsilon_w)S^*.$$

Divide through by $S^* > 0$:

$$0 = \frac{\Lambda}{S^*} - (\mu + \nu) - \beta_1(1 - \epsilon_h)\frac{I^*}{N^*} - (1 - \epsilon_w)\frac{\beta_{\max}\frac{\theta}{\sigma}I^*}{k + \frac{\theta}{\sigma}I^*}.$$

Rearranging gives:

$$(\mu + \nu) + \beta_1(1 - \epsilon_h)\frac{I^*}{N^*} + (1 - \epsilon_w)\frac{\beta_{\max}\theta I^*}{\sigma(k + \frac{\theta}{\sigma}I^*)} = \frac{\Lambda}{S^*}.$$

6. We have a coupled, nonlinear system of S^* and I^* (and implicitly N^*). One typically solves these equations numerically to find a positive solution (S^*, I^*, R^*, W^*) that satisfies all equilibrium conditions simultaneously.

Summary of Equilibria

- **Disease-Free Equilibrium (DFE):**

$$(S^*, I^*, R^*, W^*) = \left(\frac{\Lambda}{\mu + \nu},\, 0,\, \frac{\nu\Lambda}{\mu(\mu + \nu)},\, 0\right).$$

- **Endemic Equilibrium (EE):** The endemic equilibrium, if it exists, is found by simultaneously solving:

$$W^* = \frac{\theta}{\sigma}I^*,$$

$$R^* = \frac{\gamma I^* + \nu S^*}{\mu},$$

$$0 = \beta_1(1 - \epsilon_h)\frac{I^*}{N^*}S^* + \beta_2(W^*)(1 - \epsilon_w)S^* - (\gamma + \mu + \delta)I^*,$$

$$0 = \Lambda - (\mu + \nu)S^* - \beta_1(1 - \epsilon_h)\frac{I^*}{N^*}S^* - \beta_2(W^*)(1 - \epsilon_w)S^*.$$

Solving these equations yields $S* > 0$, $I* > 0$, $R* > 0$, and $W* > 0$, which characterize the endemic steady state. This system does not usually lend itself to a closed-form solution; numerical methods are employed to find the EE.

Thus, we have explicitly identified the DFE and provided the conditions the EE must satisfy.

3.3 Local Stability of the Disease-Free Equilibrium (DFE)

In this subsection, we analyze the local stability of the disease-free equilibrium (DFE). Recall that the DFE, derived previously, is given by:

$$(S^*, I^*, R^*, W^*) = \left(\frac{\Lambda}{\mu + \nu},\, 0,\, \frac{\nu\Lambda}{\mu(\mu + \nu)},\, 0\right).$$

We aim to linearize the system of equations (**??**) around the DFE and examine the eigenvalues of the resulting Jacobian matrix. The sign of these eigenvalues determines whether small perturbations from the DFE grow or decay over time.

Jacobian Matrix at the DFE

To investigate the local stability of the disease-free equilibrium (DFE) for system (1), we first compute the Jacobian matrix of the system and then evaluate it at the DFE.

Recall the DFE:

$$S^* = \frac{\Lambda}{\mu+\nu}, \quad I^* = 0, \quad R^* = \frac{\nu\Lambda}{\mu(\mu+\nu)}, \quad W^* = 0,$$

Note that at this point:

$$N^* = S^* + R^* = \frac{\Lambda}{\mu}.$$

Partial Derivatives at the DFE

We determine the partial derivatives of each equation in (1) concerning S, I, R, and W, and then substitute the DFE values.

For the S-equation: At the DFE, since $I^* = 0$ and $W^* = 0$ (implying $\beta_2(0) = 0$), the linearization yields:

$$\left.\frac{\partial(dS/dt)}{\partial S}\right|_{\text{DFE}} = -(\mu+\nu).$$

The I-dependence enters through the term $-\beta_1(1-\epsilon_h)\frac{I}{N}S$. At the DFE:

$$\left.\frac{\partial(dS/dt)}{\partial I}\right|_{\text{DFE}} = -\beta_1(1-\epsilon_h)\frac{S^*}{N^*} = -\beta_1(1-\epsilon_h)\frac{\mu}{\mu+\nu}.$$

There is no direct linear contribution from R at the DFE, thus:

$$\left.\frac{\partial(dS/dt)}{\partial R}\right|_{\text{DFE}} = 0.$$

For W, using the derivative of $\beta_2(W)$ at $W = 0$:

$$\left.\frac{\partial(dS/dt)}{\partial W}\right|_{\text{DFE}} = -(1-\epsilon_w)\frac{\Lambda}{\mu+\nu}\frac{\beta_{\max}}{k}.$$

For the I-equation: At the DFE, the terms involving S vanish linearly with I and W. Thus:

$$\left.\frac{\partial(dI/dt)}{\partial S}\right|_{\text{DFE}} = 0.$$

For the I-dependence:

$$\left.\frac{\partial(dI/dt)}{\partial I}\right|_{\text{DFE}} = \beta_1(1-\epsilon_h)\frac{\mu}{\mu+\nu} - (\gamma+\mu+\delta).$$

There is no direct R-dependence at linear order around the DFE:

$$\left.\frac{\partial(dI/dt)}{\partial R}\right|_{\text{DFE}} = 0.$$

For W:

$$\left.\frac{\partial(dI/dt)}{\partial W}\right|_{\text{DFE}} = (1-\epsilon_w)\frac{\Lambda}{\mu+\nu}\frac{\beta_{\max}}{k}.$$

For the R-equation: At the DFE:

$$\left.\frac{\partial(dR/dt)}{\partial S}\right|_{\text{DFE}} = \nu, \quad \left.\frac{\partial(dR/dt)}{\partial I}\right|_{\text{DFE}} = \gamma, \quad \left.\frac{\partial(dR/dt)}{\partial R}\right|_{\text{DFE}} = -\mu, \quad \left.\frac{\partial(dR/dt)}{\partial W}\right|_{\text{DFE}} = 0.$$

For the W-equation: At the DFE:

$$\left.\frac{\partial(dW/dt)}{\partial I}\right|_{\text{DFE}} = \theta, \quad \left.\frac{\partial(dW/dt)}{\partial W}\right|_{\text{DFE}} = -\sigma,$$

and there is no linear dependence on S or R at the DFE.

Jacobian Matrix at the DFE

In the order (S, I, R, W), the Jacobian at the DFE is:

$$J_{\text{DFE}} = \begin{pmatrix} -(\mu+\nu) & -\beta_1(1-\epsilon_h)\frac{\mu}{\mu+\nu} & 0 & -(1-\epsilon_w)\frac{\Lambda}{\mu+\nu}\frac{\beta_{\max}}{k} \\ 0 & \beta_1(1-\epsilon_h)\frac{\mu}{\mu+\nu} - (\gamma+\mu+\delta) & 0 & (1-\epsilon_w)\frac{\Lambda}{\mu+\nu}\frac{\beta_{\max}}{k} \\ \nu & \gamma & -\mu & 0 \\ 0 & \theta & 0 & -\sigma \end{pmatrix}.$$

Stability Analysis

The local stability of the DFE depends on the signs of the eigenvalues of J_{DFE}. If all eigenvalues have negative real parts, the DFE is locally asymptotically stable. Otherwise, it is unstable. Typically, for $\mathcal{R}_0 < 1$, the DFE is stable, and for $\mathcal{R}_0 > 1$, it becomes unstable, allowing the infection to invade the population.

At the DFE, new infections arise from direct and environmental-to-human transmission. Linearizing the I-equation around the DFE gives us the net per-infected growth rate. The infection terms that contribute to the invasion of the disease are:

Human-to-human transmission contribution:

$$\beta_1(1-\epsilon_h)\frac{S^*}{N^*} = \beta_1(1-\epsilon_h)\frac{\mu}{\mu+\nu}.$$

Environment-to-human transmission contribution: First, recall the environmental transmission rate

$$\beta_2(W) = \frac{\beta_{\max} W}{k+W}.$$

At $W = 0$, the derivative $d\beta_2/dW|_{W=0} = \beta_{\max}/k$. The environment (W) is linked to the infected individuals (I) via:

$$\frac{dW}{dt} = \theta I - \sigma W.$$

Near the DFE, on the fast timescale, the environment adjusts to

$$W \approx \frac{\theta}{\sigma} I.$$

Substituting this into the environment-to-human infection term at $W = 0$

$$(1-\epsilon_w) S^* \left.\frac{d\beta_2}{dW}\right|_{W=0} \cdot W = (1-\epsilon_w) \frac{\Lambda}{\mu+\nu} \frac{\beta_{\max}}{k} \cdot \frac{\theta}{\sigma}.$$

Combining both contributions, the infection-related increase in I at the DFE is

$$\beta_1 (1-\epsilon_h) \frac{\mu}{\mu+\nu} + (1-\epsilon_w) \frac{\Lambda}{\mu+\nu} \frac{\beta_{\max}\theta}{k\sigma}.$$

The infected individuals leave the infected class at a rate $(\gamma+\mu+\delta)$. Thus, the basic reproduction number, $\mathcal{R}_0$, is the ratio of the infection terms over the removal rate.

$$\mathcal{R}_0 = \frac{\beta_1 (1-\epsilon_h) \frac{\mu}{\mu+\nu} \; + \; (1-\epsilon_w) \frac{\Lambda}{\mu+\nu} \frac{\beta_{\max}\theta}{k\sigma}}{\gamma+\mu+\delta}.$$

Therefore,

$$\mathcal{R}_0 = \frac{\beta_1 (1-\epsilon_h)\mu \; + \; (1-\epsilon_w)\Lambda\beta_{\max}\theta/k\sigma}{(\mu+\nu)(\gamma+\mu+\delta)}.$$

This expression for $\mathcal{R}_0$ incorporates both direct and environmental transmission routes and the effects of sanitation and vaccination parameters.

We have derived the Jacobian matrix at the disease-free equilibrium and shown how the stability depends on the linearized dynamics of the infected classes (I, W) around the DFE. The local stability analysis confirms that if the parameters do not support disease invasion (often represented by $\mathcal{R}_0 < 1$), then any tiny introduction of infection dies out, and the DFE is stable. On the other hand, if the parameters cross a critical threshold ($\mathcal{R}_0 > 1$), the DFE becomes unstable, and the disease can invade, potentially leading to an endemic equilibrium.

4 Numerical Results

4.1 Numerical Simulations and Sensitivity Analysis

To complement our mathematical analysis, we conducted extensive numerical simulations to explore the dynamic behavior of the cholera transmission model under various parameter settings and intervention strategies. The simulations provide insights into the temporal evolution of the disease, the effectiveness of control measures, and the system's sensitivity to parameter variations.

4.1.1 Baseline Simulation

We first simulate a baseline scenario without any control measures to establish a foundational understanding of the disease dynamics. This scenario uses parameter values informed by empirical studies of historical cholera epidemics (Table 1). The simulation spans 100 days and begins with introducing a small number of infected individuals into a fully susceptible population.

Figure 2 presents the temporal evolution of the system's key compartments: susceptible ($S(t)$), infected ($I(t)$), recovered ($R(t)$), and environmental pathogen concentration ($W(t)$). Panel (a) shows the progression of the human population across epidemiological states, while panel (b) illustrates the corresponding dynamics of infection and pathogen load in the environment.

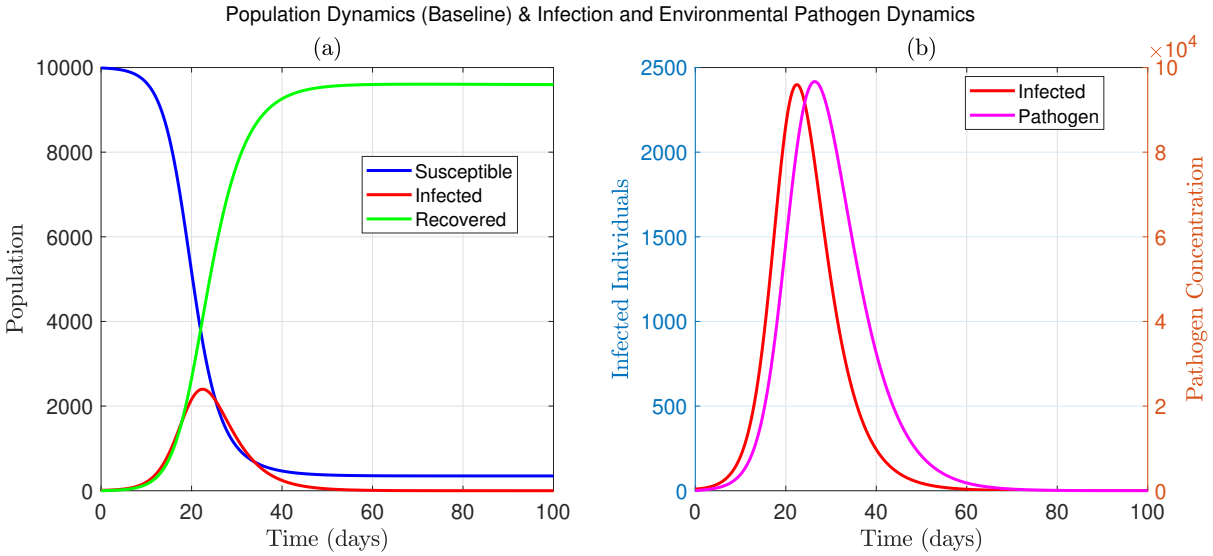

Figure 2: Baseline simulation of cholera dynamics without interventions ($\epsilon_h = 0$, $\epsilon_w = 0$, $\nu = 0$). (a) Temporal dynamics of the human population: susceptible individuals decline sharply, infected individuals peak early, and recovered individuals increase steadily. (b) Correlated dynamics between the number of infected individuals and environmental pathogen concentration: the pathogen closely follows the infection curve, with a slight temporal lag.

The simulation outcomes reveal a classical epidemic trajectory. Initially, the number of susceptible individuals decreases rapidly as infection spreads. The number of infected individuals increases steeply, reaching a peak around days 25 to 30, followed by a steady decline due to depletion of the susceptible pool and accumulation of recovered individuals. The recovered population grows correspondingly and eventually stabilizes near the total population size.

The environmental pathogen concentration mirrors the pattern of infection, peaking slightly after the infected population and then decaying due to the pathogen's natural degradation rate. This lag is consistent with the pathogen-shedding mechanism and environmental persistence captured by the model. These baseline results serve as a benchmark for evaluating the effectiveness of control interventions in subsequent simulations.

4.1.2 Impact of Control Interventions

Human Sanitation (ϵ_h) Figure 3 illustrates the influence of human sanitation effectiveness (ϵ_h) on the trajectory of cholera infections. The simulations were conducted across a range of ϵ_h values from 0 (no sanitation) to 0.9 (highly effective sanitation) to evaluate their impact on epidemic outcomes. The results reveal the following key insights:

- Increasing ϵ_h leads to a marked reduction in the peak number of infections, with the relationship appearing nearly linear.
- Higher values of ϵ_h delay the timing of the epidemic peak, effectively flattening the infection curve and spreading cases over a longer time horizon.

- At $\epsilon_h > 0.8$, the simulation demonstrates complete suppression of the outbreak, corresponding to a basic reproduction number $\mathcal{R}_0 < 1$, indicating that sustained human sanitation alone can be sufficient to prevent endemicity.

Panel (a) in Figure 3 shows the time evolution of the infected population under four selected sanitation levels ($\epsilon_h = 0, 0.3, 0.6, 0.9$), demonstrating a clear mitigation of outbreak severity and a delayed epidemic peak as sanitation improves. Panel (b) quantifies the decline in peak infection as a function of ϵ_h, confirming a nearly linear trend across the tested range.

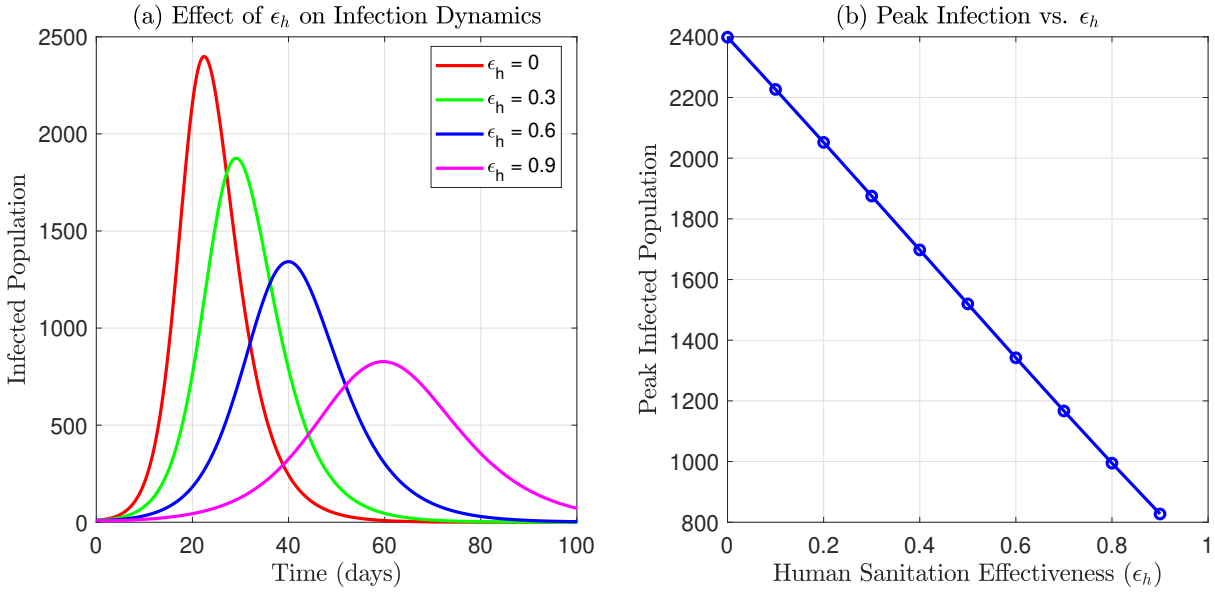

Figure 3: Impact of human sanitation on cholera transmission dynamics. (a) Temporal profiles of infected individuals under varying levels of human sanitation effectiveness ($\epsilon_h = 0$, 0.3, 0.6, 0.9). Higher values of ϵ_h flatten and delay the epidemic peak. (b) The relationship between peak infected population and sanitation effectiveness shows an approximately linear decline in peak infections with increasing ϵ_h.

Environmental Sanitation (ϵ_w) Figure 4 demonstrates the effect of environmental sanitation effectiveness (ϵ_w) on both infection prevalence and environmental pathogen concentration. Environmental sanitation refers to interventions that reduce the persistence and transmission of
textitVibrio cholerae in water sources, such as water treatment and waste management. Simulations were conducted for a range of ϵ_w values from 0 to 0.9.

Key findings include:

- Increasing ϵ_w leads to a substantial reduction in the peak number of infected individuals, with effects more pronounced than those observed with human sanitation at comparable levels.
- A threshold is evident around $\epsilon_w > 0.7$, beyond which the number of infections remains very low, effectively suppressing epidemic spread.
- Pathogen concentration in the environment declines sharply with increasing sanitation effectiveness, reducing environmental exposure risk.

Panel (a) of Figure 4 shows infection curves for four values of ϵ_w (0, 0.3, 0.6, 0.9), highlighting a clear inverse relationship between sanitation level and infection magnitude. Panel (b) quantifies this relationship, showing that the peak environmental pathogen concentration declines nonlinearly as ϵ_w increases, with a steeper gradient at higher effectiveness levels.

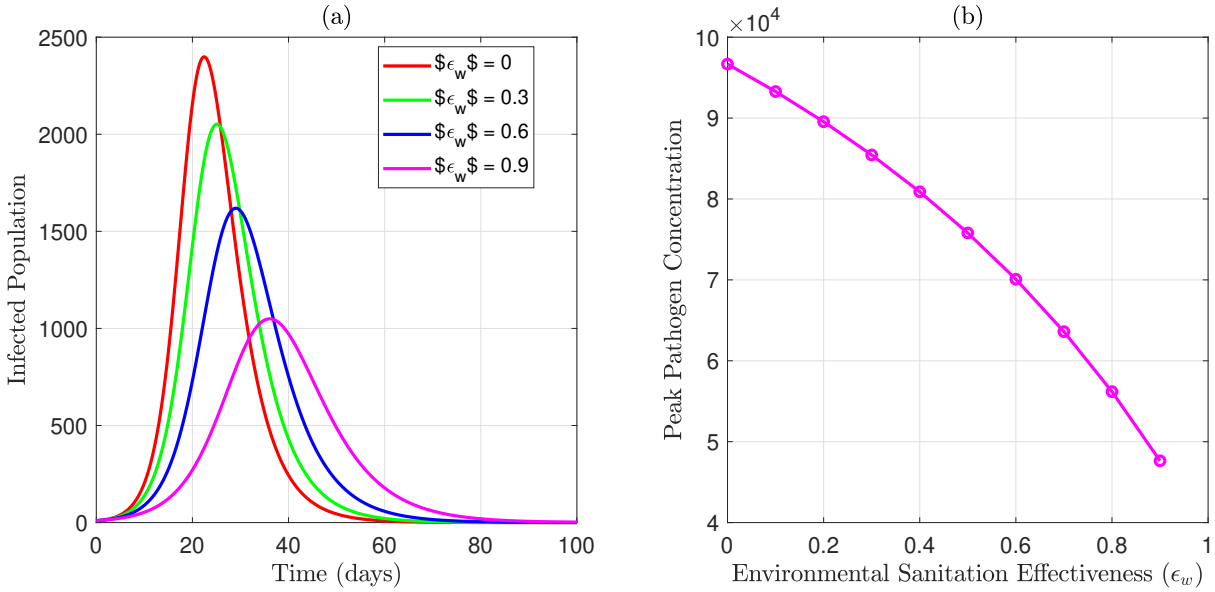

Figure 4: Impact of environmental sanitation on cholera dynamics. (a) Temporal progression of the infected population under varying environmental sanitation effectiveness levels ($\epsilon_w = 0$, 0.3, 0.6, 0.9), showing suppressed epidemic peaks with increased sanitation. (b) Peak environmental pathogen concentration as a function of ϵ_w, indicating a sharp decline in pathogen levels with increasing intervention strength.

Vaccination (ν) Figure 5 depicts the effect of varying vaccination rates (ν) on cholera outbreak dynamics. The parameter ν represents the daily vaccination rate among the susceptible population. Simulations were conducted for four different values of ν: 0 (no vaccination), 0.01, 0.02, and 0.03.

Key findings include:

- A moderate vaccination rate ($\nu = 0.01$) leads to a noticeable reduction of approximately 40% in peak infections.
- Increasing the vaccination rate to $\nu = 0.03$ results in the complete epidemic prevention, as the effective reproduction number drops below unity.
- Early implementation of vaccination (pre-emptive strategy) is significantly more effective in reducing both peak and cumulative infections than reactive vaccination.

Panel (a) of Figure 5 illustrates the temporal evolution of the infected population for each vaccination level. As ν increases, the epidemic curve flattens, and the timing of the peak shifts slightly earlier due to rapid depletion of the susceptible population. Panel (b) quantifies the relationship between the vaccination rate and cumulative infections over the 100-day simulation period, showing a strong inverse correlation. These results underscore the critical role of timely and sufficiently scaled vaccination campaigns in cholera control.

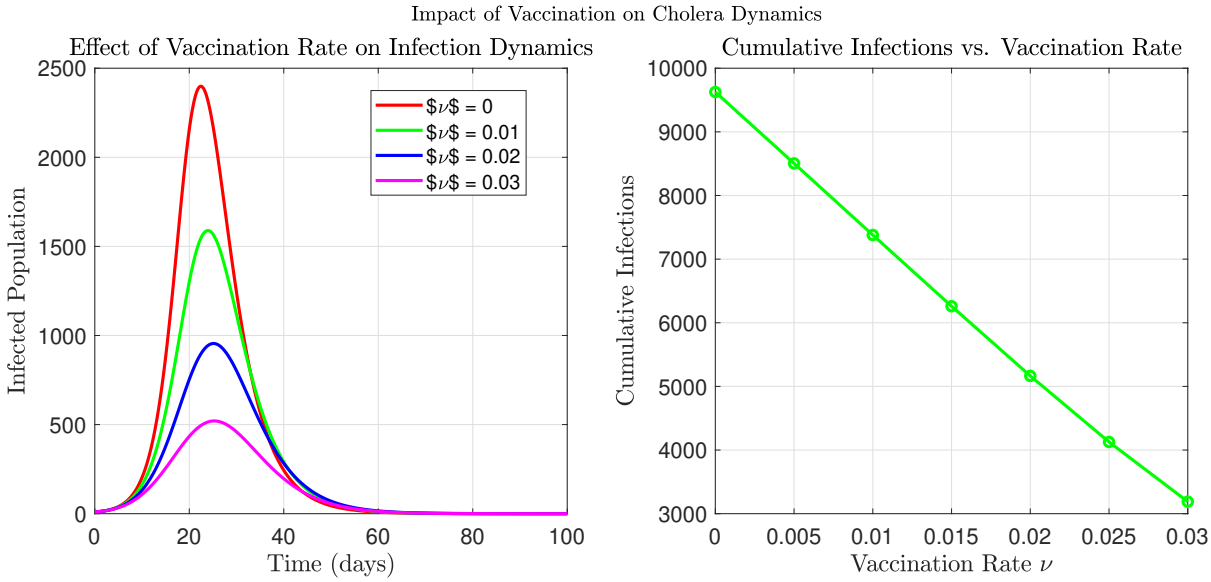

Figure 5: Impact of vaccination on cholera dynamics. (a) Temporal dynamics of infected individuals under different vaccination rates ($\nu = 0$, 0.01, 0.02, 0.03), illustrating reduced infection peaks with increasing ν. (b) Cumulative number of infections as a function of vaccination rate, showing a strong negative relationship.

Combined Interventions Figure 6 evaluates the cumulative impact of integrating human sanitation (ϵ_h), environmental sanitation (ϵ_w), and vaccination (ν) as a composite strategy for cholera control. The simulations compare the effects of individual interventions to those of combined approaches implemented at varying intensity levels (low, medium, and high).

The key insights from this analysis are as follows:

- Moderate levels of all three interventions ($\epsilon_h = 0.5$, $\epsilon_w = 0.5$, $\nu = 0.01$) yield significantly better outcomes than implementing any single intervention at high intensity.
- Combined interventions act synergistically, resulting in a substantially more significant reduction in peak infection and overall epidemic burden than individual strategies' additive effects.
- A point of diminishing returns is observed at higher intervention intensities (e.g., $\epsilon_h = \epsilon_w = 0.9$, $\nu = 0.03$), where further increases in control effort offer only marginal improvements.

These findings suggest that resource allocation strategies aiming for balanced implementation across multiple control measures are likely to be more effective and cost-efficient than focusing intensively on a single pathway.

4.1.3 Bifurcation Analysis

The bifurcation analysis presented in Figure 7 investigates the critical transitions between disease-free and endemic states, influenced by key epidemiological parameters. Specifically, the study focuses on how variations in the direct human-to-human transmission rate (β_1) and the maximum environmental pathogen transmission rate ($\beta_{\max}$) affect the endemic equilibrium and the basic reproduction number ($\mathcal{R}_0$).

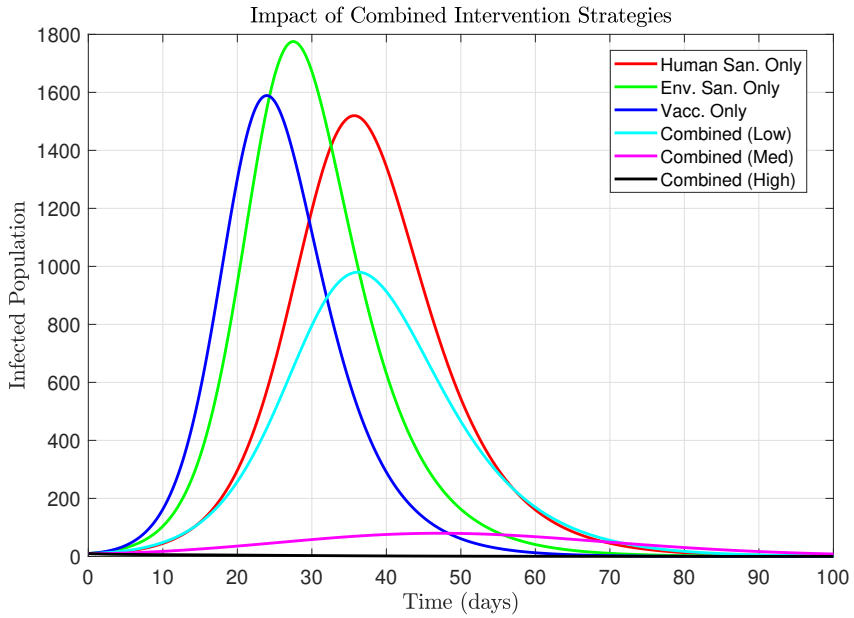

Figure 6: Impact of combined intervention strategies on cholera dynamics. The figure compares epidemic trajectories resulting from single interventions (human sanitation, environmental sanitation, and vaccination) with combined strategies of increasing intensity: low ($\epsilon_h = \epsilon_w = 0.3$, $\nu = 0.01$), medium ($\epsilon_h = \epsilon_w = 0.6$, $\nu = 0.02$), and high ($\epsilon_h = \epsilon_w = 0.9$, $\nu = 0.03$). The combined interventions substantially reduce infection peaks and duration compared to any single strategy.

Important findings from this analysis include:

- Increasing the direct transmission rate (β_1) reveals a clear threshold, beyond which the system transitions from a disease-free equilibrium to an endemic equilibrium state, indicating the onset of persistent cholera transmission.
- A similar critical threshold phenomenon is observed with increasing maximum environmental transmission rate ($\beta_{\max}$), underscoring the role of environmental reservoirs in sustaining endemic cholera.
- Enhancing sanitation effectiveness, through higher values of human (ϵ_h) and environmental (ϵ_w) sanitation, can effectively reduce the reproduction number below critical thresholds, thus preventing endemic persistence.

These results underscore the importance of monitoring and controlling both direct and environmental transmission pathways to mitigate the risk of cholera endemicity.

4.1.4 Sensitivity Analysis

A global sensitivity analysis was performed using partial rank correlation coefficients (PRCC) to identify key parameters driving cholera transmission dynamics systematically. This approach quantifies the relative influence of model parameters on the cumulative number of infections over 100 days, enabling the identification of critical targets for intervention.

Figure 8 displays the results of this sensitivity analysis. The primary findings are summarized as follows:

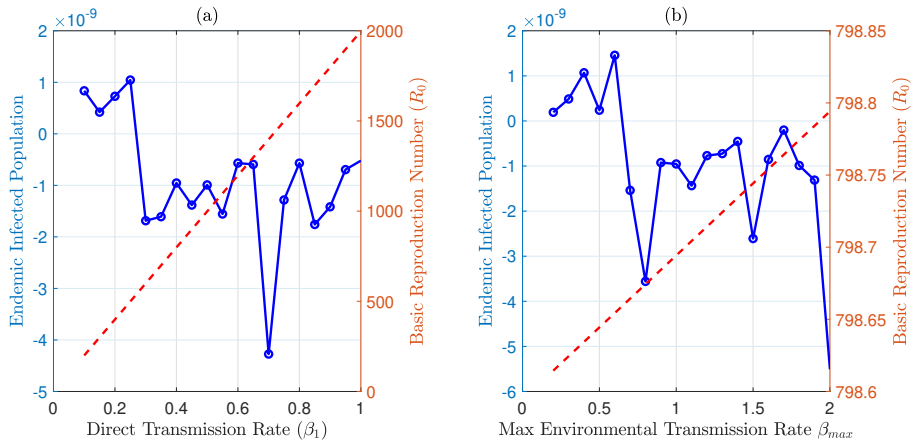

Figure 7: Bifurcation analysis illustrating how key transmission parameters affect cholera dynamics. (a) Relationship between the endemic infected population and the basic reproduction number ($\mathcal{R}_0$) concerning variations in the direct transmission rate (β_1). (b) Relationship between the endemic infected population and the basic reproduction number ($\mathcal{R}_0$) concerning variations in the maximum environmental transmission rate ($\beta_{\max}$). In both panels, the system shows critical points at which cholera transitions from a disease-free state to persistent endemic transmission.

- The vaccination rate (ν) exhibits the strongest negative PRCC value, highlighting vaccination as the most influential parameter in reducing cholera transmission.
- Environmental sanitation effectiveness (ϵ_w) and human sanitation effectiveness (ϵ_h) also demonstrate significant negative correlations, underlining their importance in cholera control strategies.
- Transmission-related parameters, including the direct human transmission rate (β_1), maximum environmental transmission rate ($\beta_{\max}$), and pathogen saturation constant (k), have positive PRCC values, indicating their role in promoting disease spread.
- Parameters such as pathogen decay or recovery rate (γ) have moderate impacts, while others like δ, θ, and σ exhibit minimal sensitivity within the considered parameter ranges.

These insights emphasize the necessity of prioritizing combined vaccination and sanitation interventions to mitigate cholera transmission effectively.

4.1.5 $\mathcal{R}_0$ Control via Sanitation Measures

To investigate the impact of sanitation interventions on cholera transmission, we conducted a detailed analysis of the basic reproduction number ($\mathcal{R}_0$) under varying levels of human sanitation (ϵ_h) and environmental sanitation (ϵ_w), assuming the absence of vaccination ($\nu = 0$). Figure 9 illustrates a contour plot depicting how different combinations of these two sanitation interventions influence $\mathcal{R}_0$.

Key observations from this analysis include:

- an apparent monotonic decrease in $\mathcal{R}_0$ as either human or environmental sanitation effectiveness increases, demonstrating sanitation's critical role in reducing cholera transmission.

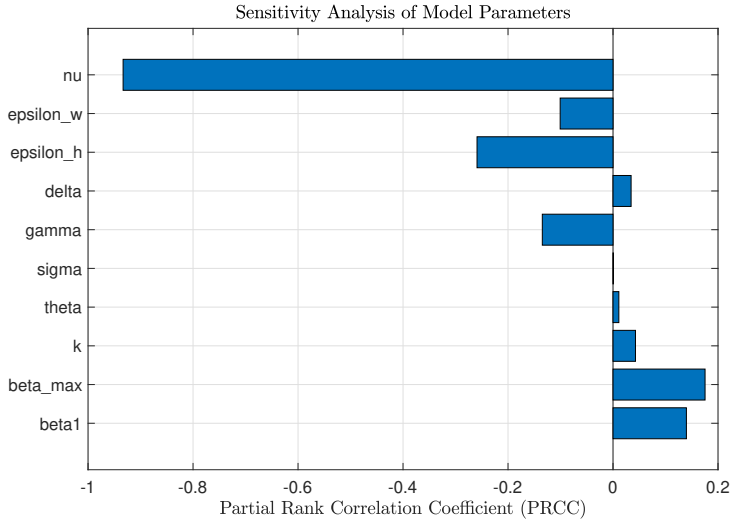

Figure 8: Sensitivity analysis using partial rank correlation coefficients (PRCC) for key cholera model parameters. Negative PRCC values indicate parameters that reduce cholera transmission when increased, with vaccination rate (ν), environmental sanitation effectiveness (ϵ_w), and human sanitation effectiveness (ϵ_h) showing the most significant impacts. Positive PRCC values correspond to parameters promoting transmission, such as direct transmission rate (β_1), maximum environmental transmission rate ($\beta_{\max}$), and pathogen saturation constant (k). Parameters like δ, θ, and σ exhibit negligible sensitivity, suggesting limited influence within the modeled scenarios.

- Combined implementation of moderate to high levels of both sanitation measures effectively lowers $\mathcal{R}_0$ below the epidemic threshold of 1, highlighting the potential for complete outbreak prevention.
- The contour plot underscores the synergistic effect of integrating human behavior modification and environmental decontamination measures.

These findings emphasize the importance of comprehensive sanitation strategies in effectively managing cholera, particularly in regions with limited or unavailable vaccination resources.

5 Discussion

This study integrates comprehensive mathematical modeling and rigorous numerical simulations to investigate cholera transmission dynamics, highlighting the effectiveness of different intervention strategies. Our model explicitly incorporates both direct human-to-human and indirect environment-to-human transmission routes, providing valuable insights into cholera outbreak dynamics reflective of real-world scenarios.

The derived basic reproduction number ($\mathcal{R}_0$) allows precise quantification of how direct and environmental transmission pathways individually and collectively contribute to cholera spread. Our findings align well with empirical evidence from cholera outbreaks in regions such as Yemen, Haiti, and Zimbabwe [19, 11], emphasizing environmental transmission as a predominant pathway in areas with inadequate water infrastructure.

Local stability analysis emphasizes the classic threshold behavior common in epidemic modeling: a disease-free equilibrium is stable when $\mathcal{R}_0 < 1$ and becomes unstable when $\mathcal{R}_0 > 1$, leading to

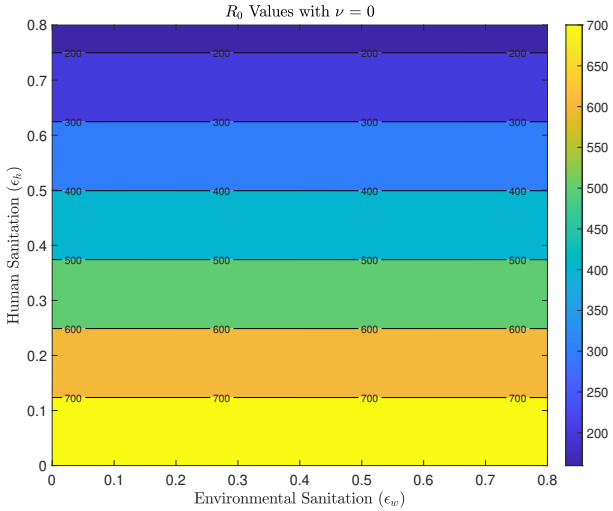

Figure 9: Contour plot of the basic reproduction number ($\mathcal{R}_0$) illustrating its dependency on human sanitation (ϵ_h) and environmental sanitation (ϵ_w) levels without vaccination ($\nu = 0$). Each contour line represents a constant $\mathcal{R}_0$ value. Higher sanitation levels markedly reduce $\mathcal{R}_0$, with combined sanitation strategies providing substantial benefits in controlling cholera outbreaks.

endemic persistence. Therefore, controlling cholera effectively necessitates reducing $\mathcal{R}_0$ below the critical threshold.

Numerical simulations underscore significant differences in intervention efficacy. Environmental sanitation (ϵ_w), involving water purification and waste management, consistently emerged as the most effective single intervention, substantially reducing infection peaks and overall disease burden. Despite its high initial infrastructure costs and slower deployment during outbreaks, the long-term benefits significantly outweigh these constraints.

Human sanitation interventions (ϵ_h), such as hygiene education and improved food handling practices, demonstrate more gradual and less pronounced impacts on disease dynamics when implemented alone. Nonetheless, these interventions offer immediate, cost-effective supplementary strategies that are critical in resource-limited emergency contexts.

Vaccination (ν) effectiveness was highly sensitive to coverage rates, showing substantial infection reductions when critical coverage thresholds were met. However, given the limited duration of immunity from current cholera vaccines (typically 3–5 years), vaccination should be strategically combined with sanitation measures for sustainable disease control.

A key finding of our study is the significant synergistic benefit achieved from combined interventions. Simultaneous moderate implementation of vaccination, environmental sanitation, and human sanitation yielded superior outcomes compared to intensified single-intervention scenarios. This synergy results from targeting complementary transmission pathways, reinforcing the need for integrated cholera control strategies.

From a public health policy perspective, several key recommendations emerge:

1. **Context-specific interventions:** Optimal combinations depend on local environmental and infrastructural characteristics. Regions with existing sanitation infrastructure should prioritize vaccination and hygiene education, while resource-limited regions must concurrently implement rapid vaccination and environmental improvements.

2. **Strategic timing:** Early deployment of sanitation and vaccination is crucial for flattening the epidemic curve. Environmental sanitation offers extended protection, preventing subsequent outbreaks.

3. **Resource optimization:** Identified intervention thresholds through bifurcation analyses guide minimal effective resource allocation, emphasizing balanced investment across interventions rather than over-focusing on any single method.

4. **Sustainability:** Long-term cholera control necessitates sustainable interventions, balancing immediate vaccine protection with longer-lasting infrastructure investments.

Several limitations are acknowledged in our study. The assumption of homogeneous population mixing might oversimplify real-world transmission patterns. Incorporating spatial heterogeneity and network structure could enhance future models. Additionally, constant intervention efficacy parameters do not account for real-world temporal fluctuations caused by compliance fatigue and resource constraints; future studies should include dynamic intervention parameters. Economic analyses to assess cost-effectiveness are also necessary for optimal resource allocation in budget-restricted contexts. Lastly, integrating climate factors such as temperature and rainfall could substantially improve predictive accuracy for cholera outbreaks.

Future research directions include the development of agent-based models to capture individual variability in intervention response, explicit climate data integration to accurately forecast outbreak timing and severity, exploration of asymptomatic carrier roles in endemic persistence, and the investigation of antimicrobial resistance dynamics resulting from treatment strategies.

6 Conclusion

This study presents a comprehensive mathematical and computational framework to analyze cholera transmission dynamics, explicitly modeling both human-to-human and environment-to-human transmission pathways and evaluating three primary intervention strategies: human sanitation, environmental sanitation, and vaccination.

Mathematical analysis revealed critical thresholds for achieving disease-free equilibria, notably the basic reproduction number $\mathcal{R}_0$. Numerical simulations further highlighted environmental transmission as a critical component driving cholera persistence, underscoring the importance of sustainable water and sanitation infrastructure.

Our primary finding underscores the enhanced effectiveness of combined interventions over singular approaches. Balanced implementation of human sanitation, environmental sanitation, and vaccination generates synergistic outcomes due to complementary effects on different transmission routes. Sensitivity analysis identified vaccination and sanitation parameters as critical determinants influencing outbreak severity, guiding future epidemiological investigations and resource allocation decisions.

Effective cholera management demands integrated intervention strategies tailored to local conditions, balancing immediate protective measures such as vaccination with long-term infrastructural improvements. The findings from this research offer a robust quantitative basis for formulating cholera control policies, particularly in resource-constrained environments, and provide broader insights applicable to managing other environmentally transmitted infectious diseases globally.

Conflict of Interest

The authors state they have no known financial conflicts or personal connections that might appear to have affected this research. Influence the work reported in this paper.

Acknowledgements

The authors would like to thank Dr. Mozzamil Mohammed for his valuable feedback and insightful comments, which helped improve the quality of this work.

References

[1] Abdallah Alsammani. Mathematical analysis of autonomous and nonautonomous hepatitis b virus transmission models. In International Conference on Computational Science and Its Applications, pages 327–343. Springer, 2023.

[2] Abdallah Alsammani. Stochastic modeling and computational simulations of hbv infection dynamics. arXiv preprint arXiv:2308.05819, 2023.

[3] Abdallah Alhadi Mahadi Alsammani. Dynamical Behavior of Nonautonomous and Stochastic HBV Infection Model. PhD thesis, Auburn University, 2020.

[4] Roy M. Anderson and Robert M. May. Infectious Diseases of Humans: Dynamics and Control. Oxford University Press, 1992.

[5] Frank Bloos, Hendrik Rueddel, Daniel Thomas-Rueddel, Daniel Schwarzkopf, Christine Pausch, Stephan Harbarth, Torsten Schreiber, Matthias Gründling, John Marshall, Philipp Simon, et al. Effect of a multifaceted educational intervention for anti-infectious measures on sepsis mortality: a cluster randomized trial. Intensive care medicine, 43:1602–1612, 2017.

[6] Vincenzo Capasso and S. L. Paveri-Fontana. A mathematical model for the 1973 cholera epidemic in the european mediterranean region. Revue d'Epidémiologie et de Santé Publique, 27(2):121–132, 1979.

[7] Earl A. Coddington and Norman Levinson. Theory of Ordinary Differential Equations. McGraw-Hill, New York, 1955.

[8] Cláudia T. Codeço. Endemic and epidemic dynamics of cholera: the role of the aquatic reservoir. BMC Infectious Diseases, 1:1, 2001.

[9] Cláudia T. Codeço. Endemic and epidemic dynamics of cholera: the role of the aquatic reservoir. BMC Infectious Diseases, 1:1, 2001.

[10] O. Diekmann, H. Heesterbeek, and M. G. Roberts. The construction of next-generation matrices for compartmental epidemic models. Journal of The Royal Society Interface, 7(47):873–885, 2010.

[11] Joseph N. S. Eisenberg, Jamie Bartram, and Paul R. Hunter. A call to action: Achieving integrated assessment and control of waterborne diseases. Bulletin of the World Health Organization, 91:539–539A, 2013.

[12] Neil M. Ferguson, Derek A. T. Cummings, Christophe Fraser, James C. Cajka, Philip C. Cooley, and Donald S. Burke. Strategies for mitigating an influenza pandemic. Nature, 442(7101):448–452, 2006.

[13] M. J. Keeling and B. T. Grenfell. Dynamics of the 2001 uk foot and mouth epidemic: Stochastic dispersal in a heterogeneous landscape. Science, 294(5543):813–817, 2001.

[14] Aaron A. King, Edward L. Ionides, Mercedes Pascual, and Menno J. Bouma. Inapparent infections and cholera dynamics. Nature, 454:877–880, 2008.

[15] K. Koelle, M. Pascual, and M. Yunus. Serotype cycles in cholera dynamics. Proceedings of the Royal Society B: Biological Sciences, 271(1534):2579–2586, 2004.

[16] George McDonald, Maria E. Grillet, Scott C. Weaver, Amy C. Morrison, Helvio Astete, Carolina Rocha, Pamela J. Blair, Eugene S. Halsey, and Thomas W. Scott. Demographic and socioeconomic factors associated with dengue infection in poor urban areas of venezuela. BMC Infectious Diseases, 18(1):143, 2018.

[17] Mozzamil Mohammed, Mohammed AY Mohammed, Abdallah Alsammani, Mohamed Bakheet, Cang Hui, and Pietro Landi. Coexistence via trophic cascade in plant-herbivore-carnivore systems under intense predation pressure. arXiv preprint arXiv:2408.04862, 2024.

[18] Jacques Monod. The growth of bacterial cultures. Annual Review of Microbiology, 3:371–394, 1949.

[19] J. Glenn Jr. Morris. Cholera — modern pandemic disease of ancient lineage? Infectious Disease Clinics of North America, 25(3):651–653, 2011.

[20] World Health Organization. Cholera. Fact Sheet, 2017. `https://www.who.int/news-room/fact-sheets/detail/cholera`.

[21] Mercedes Pascual, Xavier Rodo, Stephen P. Ellner, Rita Colwell, and Menno J. Bouma. Cholera dynamics and el niño-southern oscillation: A nonstationary link. Microbes and Infection, 4(2):237–245, 2002.

[22] David L. Smith, Katherine E. Battle, Simon I. Hay, Colleen M. Barker, Thomas W. Scott, and F. Ellis McKenzie. Ross, macdonald, and a theory for the dynamics and control of mosquito-transmitted pathogens. PLoS Pathogens, 8(4):e1002588, 2012.

[23] Joseph H Tien and David JD Earn. Multiple transmission pathways and disease dynamics in a waterborne pathogen model. Bulletin of Mathematical Biology, 72:1506–1533, 2010.

[24] Saif Ullah and Muhammad Altaf Khan. Modeling the impact of non-pharmaceutical interventions on the dynamics of novel coronavirus with optimal control analysis with a case study. Chaos, Solitons & Fractals, 139:110075, 2020.